

# Shielded Cable Transfer Impedance Measurements in the Microwave Range of 1 GHz to 10 GHz

*B. Démoulin, L. Koné, [lamine.kone@univ-lille1.fr](mailto:lamine.kone@univ-lille1.fr)*

*TELICE-IEMN Group, Université Lille 1, (France), [bernard.demoulin59@orange.fr](mailto:bernard.demoulin59@orange.fr)*

## **I. Introduction**

In the previous articles [1], [2], we have described the setup of test benches for the measurement of the transfer impedance of shielded coaxial cables. We have demonstrated that, at frequen-

cies lower than 100 MHz, a conventional triaxial setup is sufficient to make this kind of measurements. The only restrictions of its use concern practical tests performed on shielded cables with high electromagnetic immunity. In this case, it is not

unusual to come across transfer impedances the absolute value of which falls below the  $\mu\Omega/m$ . Under these conditions, the voltages of very small amplitude measured at the extremities of the test cables can be seriously perturbed by the radiation of the triaxial setup. Some adjustments were proposed with the aim of protecting the measurements from interference risks [1].

Keeping in mind that 1-m long cable samples fit very well for measurements of transfer impedances below 100 MHz, we demonstrated that in order to cover a frequency range up to 1 GHz it is necessary to reduce the cables length. Indeed, as the wavelength gets near or below the test tube dimension, propagation phenomena give rise to systematic measurement errors. In order to reduce this inconvenience, the dimension of the shield subject to the currents injected through the setup must be reduced to approximately 10 cm. Thus, this physical constraint calls for a total revision of the concept of measurement setup of transfer impedances itself.

The analysis performed in [2] mainly concerned two methods respectively based on the the wire injection method and the shield discontinuity method in a triaxial setup. Despite this improvement, the measurements reveal that at frequencies close to or superior to the GHz range, the previous methods generate new errors, this time due to the approximation of the TEM propagation. Indeed, be it the classic triaxial setup, the wire injection method or the shield discontinuity method, the transfer impedance measurement setup is based on the theory of transmission lines whose validity domain is necessarily dependent on the hypothesis of TEM signal propagation.

In order to extend the transfer impedance measurement to the microwave range, here assumed to cover the 1 GHz–10 GHz bandwidth, at the beginning of the 80's we have started to characterize the cables shielding attenuation through practical measures performed in shielded anechoic chambers. The cables, connected at both extremities to a matched load and to a spectrum analyzer installed outside the chamber, were submitted to an electromagnetic field generated by a large bandwidth antenna. This antenna, placed at 3 m distance from the cable, produces on it a local irradiation quite close to a plane-wave. The measure of the voltage amplitude gathered on the spectrum analyzer provides a clue on the attenuation generated by the cable shield. This rather simple process nevertheless presents three main difficulties. The measures will be hardly repeatable on account of the uncertainty of the radiation diagram of the cable under test connected to the load and to the receiver through high-immunity coaxial cables. The physical contribution of the junction cables considerably influences the voltage amplitude induced on the shielding outer surface. As it is almost impossible to impose a repeatable setup configuration by means of a standard, the uncertainty becomes unacceptable. The second difficulty lies in the search for an objective reference magnitude, in the view of the shielding attenuation expressed as the ratio between two physical quantities having dimensions of voltage or power. Neither the electromagnetic field measured with a sensor, nor the power induced on a receiving antenna installed in the chamber could supply this reference. Their measures are still too dependent both on the position of the sensor and on that of the receiving antenna with respect to the transmitting antenna. They therefore do not account for viable indicators. Finally, we have to turn the shield attenuation in transfer impedance in order to compare the measurements with the results achieved below 1 GHz. The direct measurement of the induced

current on the outer shield surface could solve this issue, but it will cause huge uncertainties generated by the current collector and its connection with the outside receiver. This procedure was then abandoned.

During the same period, progress made in understanding reverberation chambers allowed to use them to measure shielded cables attenuation [4]. As we will remind in section 1, the fields generated within reverberation chambers, submitted to different methods, offer interesting ways of producing repeatable attenuation measures through shielded cables or connectors. In fact, thanks to the oversizing of chambers in relation to wavelength, the objects installed in cavities with high conductive walls gain isotropic electromagnetic behaviour. This means that they are characterized by the absence of defined directivity and polarisation. Moreover, mode stirring provides uniform average amplitude of the field throughout the whole chamber. However, the average amplitude is associated to a standard deviation that becomes constant for operating frequencies of the fields situated above a minimum value defined by the chamber dimensions. The isotropic and uniformity properties of the fields allow using the power received on an antenna installed in any place in the chamber to measure the reference level. So it becomes possible to evaluate the shielding attenuation by means of a ratio between the power received on the spectrum analyzer connected to the cable end, and the reference power captured on a broadband receiving antenna. Other advantages related to the properties of cables immersed in a reverberation chamber were added. Indeed, according to the statistics of the random data collected within a reverberation room, we have established analytical formulas which yield, through a very simple calculation, the conversion of the shielding attenuation into the transfer impedance [12].

This third article will thus be entirely devoted to the description of protocols which lead to measuring the shielding attenuation in mode stirring reverberation chambers. This conversion, given in terms of transfer impedance, will be demonstrated and then illustrated by means of examples. Section 1 will be devoted to remind us the properties of reverberation chambers. It will also include the description of the installation of shielded cables (or the connectors) in preparation for the measurement of the shielding attenuation. The reader who wants to go deeper in the physical issues can refer to specialized articles on reverberation chambers. Section 2 concerns the description of the protocols adopted to measure the attenuation of shielded cables. Section 3 will mainly address the conversion of the shielding attenuation into transfer impedance and vice-versa. Section 4 deals with the chambers calibration in view of determining their natural uncertainty margin and comparing transfer impedances taken from measures with a standard based on theory. Section 5 will show the results of different measurement performed on samples of shielded cables.

## 2. Description and Physical Features of the Mode Stirring Reverberation Chambers

### *Properties*

Reverberation chambers (RC) of rectangular shape are made up of plane-parallel shielded surrounding walls working on so called either resonant modes or eigenmodes of high order. In

fact, let us consider a completely empty chamber except for an emitting antenna which does not change the electromagnetic properties of the chamber at all. Under such <<ideal>> conditions, electromagnetic theory shows that the chamber resonates at frequencies  $f_{mnp}$  determined by the following expression:

$$f_{mnp} = \frac{c}{2} \sqrt{\left(\frac{m}{a}\right)^2 + \left(\frac{n}{b}\right)^2 + \left(\frac{p}{d}\right)^2} \quad (1)$$

In this formula,  $c$  represents the speed of light, the value of which we will set at  $3 \times 10^8$  m/s, while  $a$ ,  $b$  and  $d$  are the dimensions of the cavity. The parameters  $m$ ,  $n$ ,  $p$  represent positive integer numbers, the value of which determines the order of the resonant modes. Thus, the *fundamental resonant mode* or *the first eigenmode* corresponds to a particular choice of  $m$ ,  $n$ ,  $p$  providing the lowest frequency value  $f_{mnp}$  for which we can have a non-null field inside the chamber. So, in a chamber having dimensions  $a = 1.9$  m,  $b = 2.5$  m,  $d = 2.8$  m, the fundamental resonant mode is given by the following values  $m = 0$ ,  $n = 1$ ,  $p = 1$ . Under these conditions the expression (1) anticipates a fundamental resonant mode at 80.4 MHz.

The cavity excitation at a resonant mode is represented by a standing wave whose amplitude variation in space is expressed with sinusoidal laws. It can be shown that the sinusoid period is inversely proportional to the values of  $m$ ,  $n$ ,  $p$  relative to  $f_{mnp}$ . As a consequence, when the triplet gets much higher than unity, the periodical amplitude fluctuations of the field inside the cavity becomes spatially very dense. The chamber is then said to be working in an *overmode condition*, judging from the wavelength  $\lambda_{mnp}$  corresponding to the source frequency  $f_{mnp}$ :

$$\lambda_{mnp} = \frac{c}{f_{mnp}} \quad (2)$$

Once the excitation of the *overmode condition* is reached, it can be shown that all the metallic objects in the chamber significantly influence the field distribution. The presence of the emission antenna itself provides such a perturbation, but so do other objects such as the mode stirrer shown in Figure 1. Under these conditions we realize that the presence of metallic objects moves the field distribution away from the initial sinusoidal law. The field becomes a stochastic process, the amplitude distribution of which behaves randomly distributed within the room. Measurements and theoretical simulations of reverberation chambers

indicate that we can associate known probability distributions to the electric (or magnetic) field data. Moreover, we can demonstrate that the mode stirrer rotation can produce new sets of random data in an almost independent way. The only condition required to observe this phenomenon is that the angular spacing of the mode stirrer progressive positions be over a threshold fixed by uncorrelation criteria for the electromagnetic field.

We can then associate average amplitude with a standard deviation to the fields or to other physical data such as currents, voltages, power. A reverberation chamber properly calibrated implies that the average amplitude is independent from the position of an observer moving in a certain chamber working volume. Under these preliminary conditions, the average amplitude is associated to an uncertainty whose value equally follows a stationary behavior. In practical terms, this means that the uncertainty is independent from the chamber volume and from the physical nature of its content.

The minimum frequency from which the reverberation chamber acquires its remarkable properties depends on the characteristics of the mode stirrer and on the dimensions of the chamber setting the fundamental resonance. The frequency threshold which determines its functioning is called lowest usable frequency (LUF) or starting frequency. It is represented by the symbol  $f_s$ , which is in general approximately 5 or 6 times greater than the fundamental resonant frequency of the empty chamber. In the above example, this threshold is located between 400 and 480 MHz.

## Description

The emitting antenna Tx and the receiving broadband antenna Rx will be arranged in order to reduce their direct coupling as much as possible. The mutual coupling reduction can be eased by directive antennas of the log-periodic or horn types. However, experience tells us that some acceptable results can also be obtained with the help of antennas made up of conductors arranged at around 10 cm from the metallic walls of the chamber. The conductors so arranged form radiating transmission lines, one end of which is connected onto the broadband radio frequency source and the other end to a matched load.

With two identical antennas, the emitting one placed on one of the walls and the receiving one on the opposing wall, we can reduce their mutual coupling by a large amount. These reduced-size antennas are matched for a frequency range which goes from a hundred MHz to around 10 GHz. In exchange, their poor efficiency is balanced by the natural increase of the amplitude of standing waves produced by the chamber.

The mode stirrer, made up of metallic blades and set into rotation by an external electrical motor, is located on the top wall, but other arrangements are also possible. The control of the angular position of the mode stirrer will be set via software. The emitting source and the receiver will be placed outside the chamber. We can use a conventional generator and spectrum analyzer, but the two functions can be combined by employing a network analyzer. The installation of the cables under test (C.U.T.) requires a direct connection to the external receiver as well as a connection to a matched load placed in the chamber or connected to an external load. The discussion on which arrangement may be chosen will be undertaken in Section 5 by describing some measurement examples in RCs.

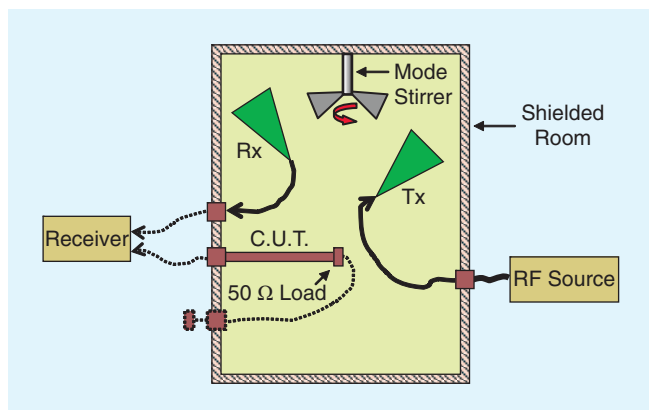


Fig. 1. Arrangement of the reverberation room to perform transfer impedance measurements.

Figure 2 adds more details to the installation of cables under test of a dimension  $\Delta L$  close to 10 cm. The sample so configured will be extended at the extremities by two pieces of high-immunity shielded coaxial cables. The dimensions of these additional cables must be bigger than the wavelength required by the lowest frequency found during measurements. For example, for 1 GHz, corresponding to a wavelength of 30 cm, the dimensions will be at least the double of  $\lambda$ , which is larger than 60 cm. It has to be remarked that the sample of the cable under test  $\Delta L$  will be placed in a zone where the average amplitude of the field is statistically uniform. Studies of reverberation chambers show that this condition is satisfied when the distance from metallic walls is at least larger than a quarter wavelength. Thus, for a minimum frequency of 1 GHz, with a distance of 7.5 cm between the walls, the field uniformity is achieved. More details about the reverberating chambers may be found in [7], [10], and [11].

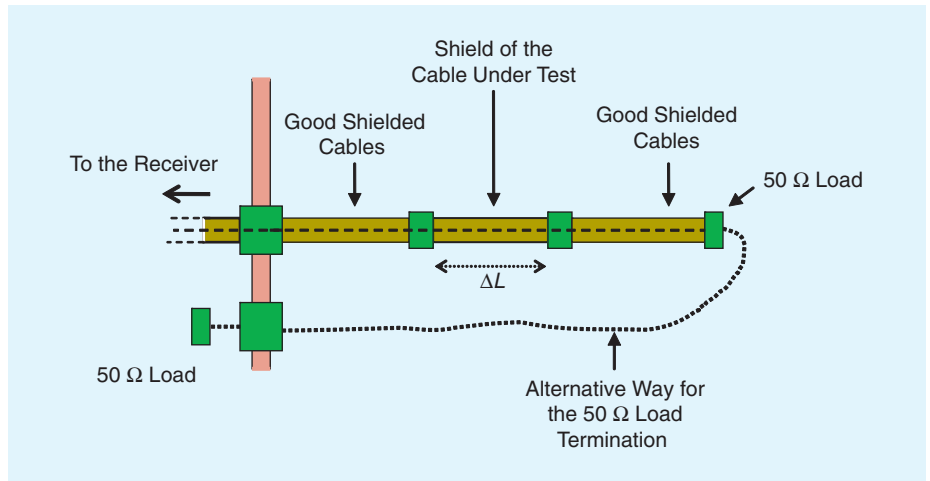


Fig. 2. Details of the Cable Under Test arrangement.

### 3. Method for the Measurement of Shielding Attenuation of a Cable Sample

The shielding attenuation measurement of the C.U.T, as described in the previous section assumes that the average amplitude of the field inside the chamber meets statistic uniformity criteria. A preliminary calibration of the chamber, for which we will mention the principle in Section 4, is suggested. In compliance with this condition and with the installation criteria described in the previous section, the attenuation measurement consists of two stages which aim at estimating the average power captured at the C.U.T's end. The term «estimate» is better suited than the term «determination» since the measurements are performed on a limited number of data, however sufficiently large and set by the minimum angular step of the mode stirrer.

#### Estimate of the Reference Average Power

On the whole frequency range explored in testing, we proceed by measuring a reference power  $P_r$ , collected on the receiver connected to the Rx antenna. During the measurement, the emission power sent to the Tx antenna can either be kept unmodified or not, according to the frequency function. Such power data will in any case be stored in order to perform the second step of the attenuation test.

For each frequency sample, we perform a rotation of the mode stirrer so as to capture  $N$  power samples  $(P_r)_i$ . The index  $i$  identifies any sample from this group  $N$ , uniformly distributed. From this measure we estimate the average amplitude  $\langle P_r \rangle$  of the reference power, as:

$$\langle P_r \rangle = \frac{1}{N} \sum_{i=1}^N (P_r)_i \quad (3)$$

The value  $N$  of samples must satisfy the condition of large numbers, that is to say the set  $N$  contains an adequate quantity

of statistically independent data. In order to fix this number we recommend referring both to the international standards such as IEC 61000-4-3 and to specialized literature on reverberation chambers [10], [11].

#### Estimate of the Power Collected on the Cable Under Test

We repeat the previous protocol with the end of the C.U.T. connected to the receiver. This time the Rx antenna is connected to a  $50 \Omega$  load, similar to the input impedance of the receiver. On the  $N$  positions of the mode stirrer we measure the power  $(P_c)_i$  collected at the cable's termination, as done before, and we estimate the average power:

$$\langle P_c \rangle = \frac{1}{N} \sum_{i=1}^N (P_c)_i \quad (4)$$

It ought to be noted that in the second stage, the power level injected on the Tx antenna must be exactly equal to the level memorized in the previous stage for every frequency sample. It follows that we turn either to a logarithmic or to a linear representation and the attenuation  $A$  given by the shielded cable sample will be expressed through the following formula:

$$\hat{A}_{\text{lin}} = \frac{\langle P_c \rangle}{\langle P_r \rangle} \quad \hat{A}_{\text{dB}} = 10 \log \left( \frac{\langle P_c \rangle}{\langle P_r \rangle} \right) \quad (5)$$

The sign  $\hat{}$  placed on top of the symbol  $A$  reminds us that the measure comes from a random process. In fact, each average estimation, as indicated in (4), is affected by an uncertainty defined by the law of large numbers. If the chamber was calibrated according to the protocol mentioned in section 4, the uncertainty should be independent from the chamber volume and the nature of its content.

In order to keep the quality coefficient of the chamber ( $Q$  factor) unchanged during the collection of power  $P_c$  by the cable under test, the receiving antenna will be connected to a load impedance similar to the input impedance of the receiver, usually  $50 \Omega$ . Without this precaution, the field amplitude

might be more or less modified, and this translates into a systematic error.

#### 4. Shielding Attenuation and Transfer Impedance Conversion

This section comprises two parts, one devoted to explaining the physical properties of wire-like objects submitted to the electromagnetic field randomly generated into a reverberation chamber. The second part is devoted to describing the protocols which help us converting the screening attenuation into transfer impedance.

##### Behaviour of Wire-Like Conductors Immersed into a Reverberation Chamber

Figure 3 represents an electric monopole connected to an infinite perfectly conducting plate with load impedance  $Z_L$ . In this figure,  $E_z(x, y, z)$  represents the electric field in the chamber, with polarization parallel to the monopole.

It can be proved that, in a properly calibrated chamber,  $E_z(x, y, z)$  behaves like a random variable. The probability distribution of the real and imaginary components follow the Gaussian distribution. Let's consider in the meantime the field  $E_z$  in any point of the surface where the monopole in Figure 3 will be placed, namely  $E_z(0, 0, z)$  with  $0 < z < L_0$ . Whenever the wavelength is much lower than  $L_0$ , the projection of the field  $E_z$  on the monopole behaves exactly as a random variable, and the same will be for the induced current  $I_M(z)$ . It can be demonstrated that the variables  $E_z$  and  $I_M(z)$  obey the ergodicity principle. That is to say, an observer set in any point of the monopole observes, as a consequence of stirrer rotation, that the amplitude of the random variables  $E_z$  and  $I_M(z)$  follow a distribution of probability similar to that observed if he moves along the  $oz$  direction of Figure 3.

In order to ease the rest of this presentation, we will think the field distribution in the chamber as due to the combination of a large number of waves converging towards the object under test [5], [10], [11]. The analysis of how a reverberation chamber physically works shows us that we can reproduce the random variable  $E_z$  as a superposition of a large number of plane waves  $N_w$  having constant amplitude  $E_w$  whose incidence angles  $\Omega_n$ , polarisation angles  $\eta_n$  and the phase angle  $\phi_n$  are distributed according to a uniform distribution, that is

$$E_z = \sum_{n=1}^{N_w} (E_w)_n \quad (6)$$

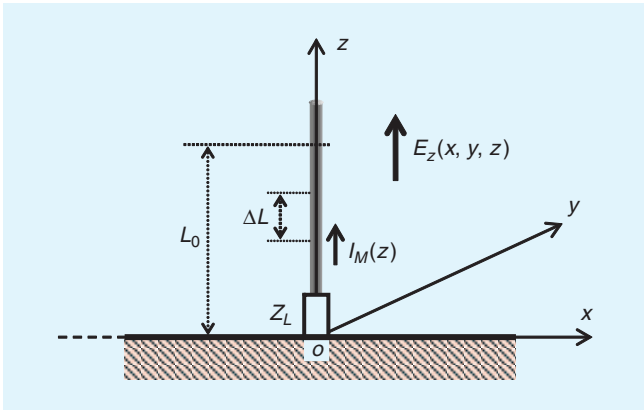


Fig. 3. Outer surface of the cable under test behaves like a short circuited electric monopole.

In the above formula, the symbol  $(E_w)_n$  represents one of the  $N_w$  plane waves of constant amplitude  $E_w$ , while  $E_z$  refers to the entire random set.

We know that when a measurement is performed on the load impedance  $Z_L$  connected to the base of the monopole of Figure 3, the average power  $\langle P_r \rangle$  collected on  $N_S$  positions of the mode stirrer will be expressed as:

$$\langle P_r \rangle = \frac{1}{N_S} \sum_{i=1}^{N_S} (P_r)_i \quad (7)$$

In this relation,  $(P_r)_i$  is equal to the power captured for any angular position  $\theta_i$  of the mode stirrer.

If we perform  $N_S$  independent realizations of the variable  $E_z$ , according to (6), it can be shown that the average power collected on  $Z_L$  for such  $N_S$  realizations can be expressed with the following formula [11]:

$$\langle P_r \rangle = \frac{E_w^2}{Z_w} \langle S_e \rangle \quad \text{where } Z_w = \sqrt{\frac{\mu_0}{\epsilon_0}} \cong 377 \Omega \quad (8)$$

In the above expression,  $E_w$  represents the amplitude of the fictitious plane waves,  $Z_w$  the plane wave impedance given by the square root of the ratio between the magnetic permeability of vacuum  $\mu_0$  and the electric permittivity of vacuum  $\epsilon_0$ , whereas the term  $\langle S_e \rangle$  is equal to the estimated average effective area of the monopole. This quantity is related to the  $N_S$  plane wave samples considered above. Knowing that the expression (8) can also be written

$$\langle P_r \rangle = Z_w \langle I_M^2 \rangle \quad (9)$$

the term  $\langle I_M^2 \rangle$  represents the mean square amplitude estimate of the current  $I_M$  induced on the monopole for the previous  $N_S$  plane waves configurations. If we apply this argument to the cables under test, the extremity of which opposite to the chamber wall is left in open circuit, namely without the link marked by the dotted line in Figure 2, the current  $I_S$  induced on the shielding is thus similar to the current induced on the monopole in Figure 3 short circuited to the base, being  $Z_L = 0$ .

As the dimensions  $L_0$  of the monopole or of the cable under test exceed the wavelength, and if we assume a constant value for the average amplitude of the field in the chamber, the average square values of  $I_M$  and  $I_S$  calculated on  $N_S$  plane wave realizations or  $N_S$  positions of the mode stirrer finally converge to identical values, hence:

$$L_0 \gg \lambda \quad \text{and} \quad E_w = \text{const} \rightarrow \langle I_M^2 \rangle = \langle I_S^2 \rangle \quad (10)$$

If  $P_c$  represents the power collected on the extremity of the cable under test (C.U.T.), the formula becomes:

$$\langle P_c \rangle = \frac{E_w^2}{Z_w} \langle S'_e \rangle \quad \text{with} \quad \langle S'_e \rangle \ll \langle S_e \rangle \quad (11)$$

This equation can be rephrased after the insertion of the term  $\langle I_S^2 \rangle$  introduced in (10) and of an impedance term  $Z_w'$  which remains to be determined.

$$\langle P_c \rangle = Z_w' \langle I_S^2 \rangle \quad (12)$$

As we know that the sections situated on either side of the sample under test have a dimension larger than the wavelength  $\lambda$ , but the dimension  $\Delta L$  of the shielding under test remains smaller than  $\lambda$ ,  $\langle P_c \rangle$  can be written:

$$\langle P_c \rangle = \frac{1|Z_t|^2}{2 Z_c} (\Delta L)^2 \langle I_s^2 \rangle \quad \text{where } Z_L' = Z_c \quad (13)$$

In this formula, the term  $Z_t$  represents the transfer impedance of the cable under test, whereas the term  $Z_c$  means that the cable's load impedance  $Z_L$  is matched to its own characteristic impedance  $Z_c$ .

Thus, we can determine the link between the shielding attenuation measure, as it is defined by the formula (5), and the transfer impedance.

### Physical Principle of the Conversion of Shielding Attenuation into Transfer Impedance

As long as the dimension of the receiving antenna used for measuring power is larger than the wavelength, the average power  $\langle P_r \rangle$  will be equal to the power collected on load impedance  $Z_L$  on the monopole in Figure 3. Consequently, if we take the ratio between (13) and (9), the result is very similar to the shielding attenuation described in (5), hence:

$$\frac{\langle P_c \rangle}{\langle P_r \rangle} = \frac{1|Z_t|^2}{2Z_cZ_w} (\Delta L)^2 \frac{\langle I_s^2 \rangle}{\langle I_M^2 \rangle} = \hat{A}_{\text{lin}} \quad (14)$$

Using the mean square estimate of the current amplitude as expressed in (10), we will easily find the conversion formula we were looking for:

$$|\hat{Z}_t| = \frac{\sqrt{2Z_cZ_w}}{\Delta L} \hat{A}_{\text{lin}} \quad (15)$$

When the attenuation is expressed in dB, the above equation becomes:

$$|\hat{Z}_t| = \frac{\sqrt{2Z_cZ_w}}{\Delta L} 10^{+0.05\hat{A}_{\text{dB}}} \quad (16)$$

The sign  $\hat{}$  placed on top of the symbol  $Z_t$  means that the determination of the transfer impedance is necessarily affected by the uncertainty related to the estimation of  $A_{\text{lin}}$  or  $A_{\text{dB}}$ . It's worth remembering that the terms  $Z_c$  and  $Z_w$  which appear in those formulas represent in turn the characteristic impedance of the cable under test (C.U.T.) and the impedance of the plane wave defined in (8). Some details about the transfer impedance conversion may be found in standard IEC 61196-1-4 or in [11].

## 5. Determination of the Uncertainty Margin and Calibration of the Transfer Impedance Measurement

In this section we will first of all examine the calibration procedure of the intrinsic margin of error in a reverberation chamber. In determining this parameter we will stick to standard specifications. Then we will perform the actual calibration of the transfer impedance, by using a shielded sample with a single small aperture as described in a previous paper [2].

### Margin of Error Calibration

Let us now verify, by using an appropriate measurement procedure, that the electromagnetic field amplitude, as it is distributed in the reverberation room, is statistically uniform. In order to perform repeatable measures it is essential to adhere to this condition. By reproducible measures we mean data, of shielding

attenuation or transfer impedance, extracted from measurements whose results are independent from the chamber's volume. We will only mention the physical principle of the calibration procedure, while readers wishing to have more details will need to refer to reverberation chambers regulations as found in standard IEC-61000-4-3 or to specific literature [10], [11].

Figure 4 offers a representation of the chamber specifically configured for calibrating the margin of error on the working volume edges delimited by the parallelepiped drawn within the chamber with a dotted line. Using a field sensor which delivers the absolute amplitude of the three cartesian components  $E_{xyz}$ , we estimate, on each of the 8 points A, B, C, D, E, F, G, H, the field's average amplitude collected on  $N_s$  angular positions of the stirrer:

$$\langle (|E_x|)_A \rangle = \frac{1}{N_s} \sum_{i=1}^{N_s} (|E_x|)_i \quad (17)$$

We will repeat this average estimate on all 24 combined configurations of position and polarization, hence:

$$\langle E \rangle = \frac{1}{24} [\langle (|E_{xyz}|)_A \rangle + \langle (|E_{xyz}|)_B \rangle + \dots + \langle (|E_{xyz}|)_H \rangle] \quad (18)$$

According to the notation in (18), we will write:

$$\langle (|E_{xyz}|)_A \rangle = \langle (|E_x|)_A \rangle + \langle (|E_y|)_A \rangle + \langle (|E_z|)_A \rangle \quad (19)$$

Then we will estimate the variance as:

$$\langle \sigma_E^2 \rangle = \frac{1}{24} [ \langle (E_x)_A - \langle E \rangle \rangle^2 + \dots + \langle (E_z)_H - \langle E \rangle \rangle^2 ] \quad (20)$$

Expression (20) will be computed for each polarization  $x, y, z$  of the sensor and at each corner point A, B, C, D, E, F, G, H of the working volume [11].

After correcting the bias error, we get to the variance adopted for calculating the standard deviation of the field  $\sigma_E$ , [11].

$$\hat{\sigma}_E^2 = \frac{24}{24-1} \langle \sigma_E^2 \rangle \rightarrow \hat{\sigma}_E = \sqrt{\hat{\sigma}_E^2} \quad (21)$$

If  $S_\sigma$  indicates the ration between the relative standard deviation and the estimate of the average amplitude, we will have:

$$S_\sigma = \frac{\langle E \rangle + \hat{\sigma}_E}{\langle E \rangle} \quad \text{or} \quad (S_\sigma)_{\text{dB}} = 20 \log(S_\sigma) \quad (22)$$

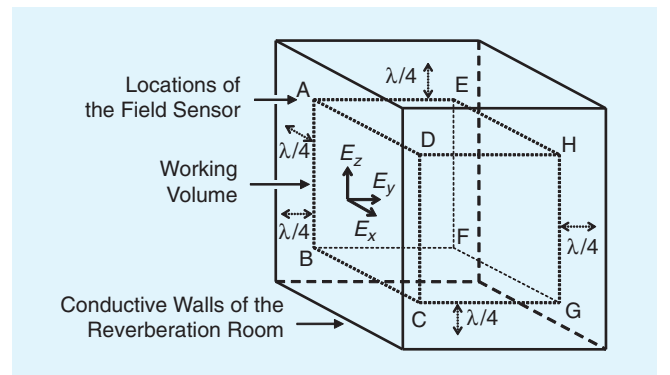


Fig. 4. View of the reverberation room to perform the field uniformity test at 8 corners of the working volume as drawn with thin dotted lines.

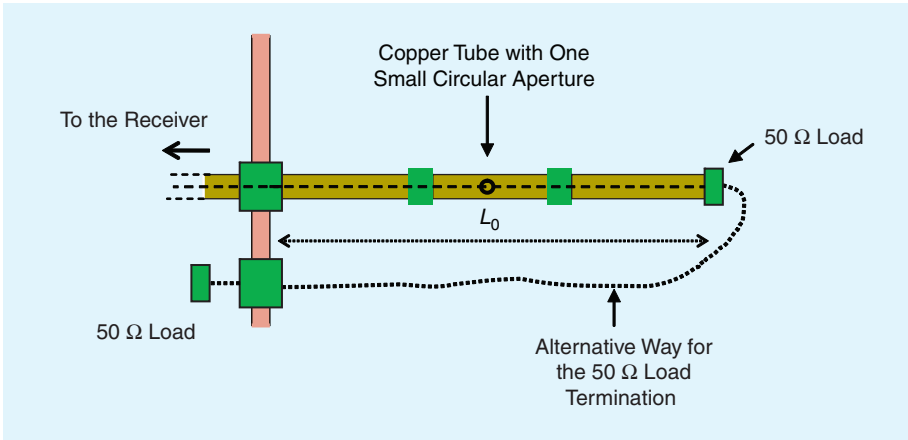


Fig. 5. Coaxial cable with one small aperture used for the relative calibration in reverberation room. The total length  $L_0$  must be oversized in respect of the wavelength,  $L_0 \gg \lambda$ .

A chamber complying with the statistical uniformity criteria of the field as set by the standards, will have to show, at the time of the calibration, a relative standard deviation  $S_\sigma$  or ( $S_\sigma$ ) dB lower or at most equal to a normalized margin gap. This condition has to be verified for the entire frequency range explored while measuring the shielding attenuation.

A reverberation chamber satisfying the requirement of the normalized margin gap must in principle provide a uniform average field within the working volume delimited by the dotted lines in Figure 4. We ought to remember that the boundaries of the working volume are placed at a minimum distance from the chamber walls that is equal or larger than a quarter of the wavelength. If we take a look at Figure 1, we see that the device under test will not be entirely contained in the working volume, as the connection(s) made with the external receiver (and load) will experience a non-uniform field area situated near the walls. Nevertheless, as the total dimension  $L_0$  of the device under test is larger than the wavelength, it can be proved that this imperfection does not influence the quality and reproducibility of the measures. The most important criterion requires that the position of the cable shielding of dimension  $\Delta L$  is well fit into the working volume.

The uniformity calibration of the field is optional, since this procedure is generally carried out periodically by chambers' maintenance teams or exceptionally when tests on bulky or electromagnetically absorbing objects are carried out. The cables or the connectors interested by shielding attenuation measurements do not belong in this frame.

Since we are dealing with relative measurements, the calibration of the error margin is less important than for tests of immunity, susceptibility, or radiated emissions. However, if in doubt, performing the error margin test allows us to better identify the lowest usable frequency (LUF) of the chamber. The empirical rule set for the LUF is, that  $f_s$  must be 4 or 5 times the frequency of the fundamental mode of the empty chamber.

### Transfer Impedance Measurement Calibration

The procedure adopts a coaxial sample with a small aperture. Let us remind you that the physical principle of this device has to a large extent been explained in a previous paper [2].

The sample will be connected at both extremities to two samples of high-immunity coaxial cables. In Figure 5 the installation details in relation to the chamber's metallic walls are given.

The calibration consists in providing the measurement of the screening attenuation described in Section 2. Then we go on to the conversion of the attenuation into transfer impedance through formulas (15) and (16). These expressions, valid for a uniformly distributed coupling, will yet have to be transformed for the isolated coupling given by the sample aperture in Figure 5. In this case, the transfer impedance will be identified by the symbol  $Z_{i0}$  and the

term  $\Delta L$  will be deleted, hence:

$$|\hat{Z}_{i0}| = \sqrt{2Z_c Z_w} \hat{A}_{in} |\hat{Z}_{i0}| = \sqrt{2Z_c Z_w} 10^{+0.05\hat{A}_{dB}} \quad (23)$$

At the frequencies considered, and with reference to [2], we know that  $Z_{i0}$  assumes the following approximate value:

$$Z_{i0} \cong j L_{i0} \omega \quad (24)$$

In this formula,  $L_{i0}$  represents the transfer inductance of the sample. The calculations performed in [2] allow us to evaluate the theoretical value of  $Z_{i0}$  dependent on the diameter  $D$  of the sample tube and the diameter  $d$  of the aperture. The calibration procedure involves comparing the theoretical curve calculated by (24) with the  $Z_{i0}$  experimental curve derived from the shielding attenuation measure, thanks to the transformations drawn from (23).

## 6. Examples of Measurements Carried Out in Reverberating Chamber

Measurements involve in turn a calibration sample including a small circular aperture and a single braid coaxial cable sample, bearing the commercial reference RG-58. The tests will be performed in a reverberation room having 6.5 m  $\times$  4 m  $\times$  2.8 m dimensions and 72 m<sup>3</sup> volume, the fundamental mode of which (first eigenmode) is located at 40 MHz and with a lowest usable frequency (LUF)  $f_s$  at around 200 MHz. The transmitting antenna Tx, as well as the receiving antenna used to measure the reference power, is of log-periodic type up to a 3 GHz, while from 3 GHz to 10 GHz we use a wideband horn antenna.

### Measurements Performed on a Calibration Sample

The calibration sample is made up of a brass tube having an external diameter of 12 mm and a 1 mm thickness. This tube forms a coaxial pipe, the characteristic impedance of which is very close to 50  $\Omega$ . On the shielding surface an aperture of diameter  $d$  of 5 mm is made, in order to produce the electromagnetic coupling described in [2] and [3].

The test sample is placed in the chamber according to the setup described in Figure 5. The tests have shown that the

conductor link (marked with a dotted line on this figure) has no influence provided that the frequency exceeds  $f_s$ , which is 200 MHz. Figure 6 shows different curves which allow us to find the transfer impedance of the sample from the shielding attenuation by means of the conversion rules described in detail in section 3.

The green curve of Figure 6 provides the evolution of the transfer impedance extracted from (23). The frequencies explored by the measurement range from 30 MHz to 10 GHz, and the dashed vertical line sets the LUF of the chamber. Consequently, only the part of the curve situated above  $f_s$  is currently usable. Nonetheless, examining the trends on either side of  $f_s$  gives us interesting comments on the physical behavior of a reverberation chamber. In fact, at frequencies close to 40 MHz, we can observe an important amplitude fluctuation of  $Z_t$ , linked to the chamber's fundamental resonance, predicted by (1) to be positioned at 40 MHz. From 40 MHz to 200 MHz, the fluctuations decrease but remain important, and this seems to prove that the statistical properties of the field distribution in the chamber are not completely acquired. On the other hand, above 200 MHz the uncertainty margin is reduced and becomes stationary, thus proving that the chamber conforms to the expected behavior.

The blue curve of Figure 6 refers to the theoretical characteristic deduced from (24) in which the transfer inductance  $L_t$  is computed thanks to expression (19) of [2] and reminded below:

$$L_t = \frac{\mu_0 \alpha_m}{\pi^2 D^2} \quad (25)$$

Knowing that for a circular opening the magnetic polarizability  $\alpha_m$  is expressed by

$$\alpha_m = \frac{d^3}{6} \quad (26)$$

the theoretical transfer inductance of the sample tube takes a value of  $1.8 \cdot 10^{-2}$  nH.

The red curve of Figure 6 corresponds to the transfer impedance as deduced from the measurements by means of the shielding discontinuity method described in [2].

By comparing these results we see a very satisfactory correspondence within the range 200 MHz to 1 GHz. By contrast, above 1 GHz the transfer impedance derived from the shielding attenuation measurement in the reverberation chamber, shows a rise which is higher than the linear law with frequency as predicted by (24). The reasons behind this gap are still not clear. We consider the possible contribution of the three phenomena. Indeed, the transfer inductance as it is presented in (25) is calculated under the hypothesis of the transmission line theory. This means that  $L_t$  represents a mutual coupling coefficient between a transmission line external to the test tube and the coaxial line to the test structure itself [6]. On the other hand, the approach adopted in section 3 to convert the shielding attenuation into transfer impedance outclasses the concept of mutual coupling.

Certainly, in this argument it is accepted that the power collected on the calibration sample is connected to the quadratic norm of the current induced on the shielding outer surface by means of a proportionality factor which is similar to the transfer impedance. This point deserves to be considered in depth. On the other hand, it is possible that the rise observed from 1 GHz is stimulated by a physical evolution of coupling phenomena

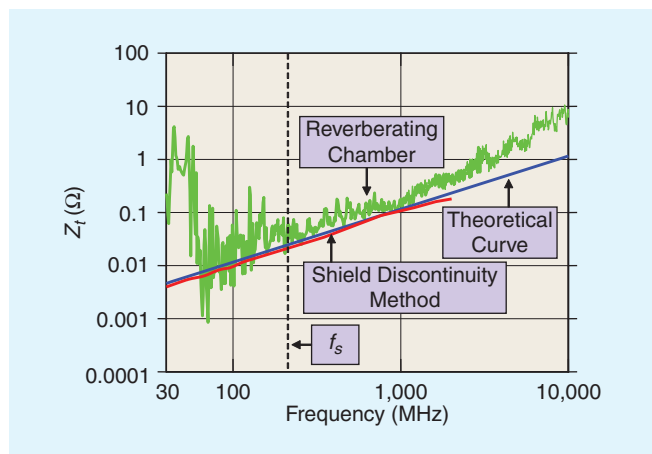


Fig. 6. Measurements carried out on a calibration sample with one small aperture (green curve) in a reverberation chamber. The measurements are compared with the theoretical curve of transfer impedance (blue curve) and other measurements performed with the shield discontinuity method on measurement setup (red curve).

already present below 1 GHz, the contribution of which might become crucial in the microwave frequency range.

In a theoretical work in 1993, F. Broyd  [8] has introduced five coupling modes for electromagnetic fields which operate on a shielded cable. Certain phenomena assume the concept of mutual coupling like the transfer impedance and the transfer admittance as used by the transmission lines theory. Others are manifestly unrelated to this context, in particular the couplings introduced by the magnetic field component perpendicular to the aperture or parallel to the longitudinal axis of the sample. Finally, a third physical cause might come from a direct electromagnetic coupling due to the far-field radiation of the aperture made on the calibration sample shield.

In order to have a better understanding, let us use reciprocity with the source connected to one extremity of the sample, while the other extremity is matched at  $50 \Omega$ . Under these conditions, the electromagnetic field radiated outside of the sample is the result of the superposition of two phenomena. A direct field due to radiation of the equivalent magnetic dipole of the aperture, and an indirect field coming from the radiation of the current induced by the aperture in close proximity and flowing on the outer surface of the cable shield. This current must in principle match with the concept of transfer impedance introduced in section 3, where the conversion protocol was illustrated. Y. Bourri [9] has recently shown that above 1 GHz the indirect coupling mostly appears at the sample resonance, while outside of such frequencies, it is the direct coupling which controls the cable radiation. A thorough analysis of these phenomena applied to the current measurement setup will undoubtedly allow us to strengthen our interpretation.

### Measures Performed on a Single Braid Shielded Cable

The curves presented in figure 7 provide us with the transfer impedance characteristics measured on a cable sample RG-58 of a dimension  $\Delta L$  reduced to 10 cm. The installation of the sample was carried out in accordance with the specifications in figure 2, as before; with the device extremity left open. In the

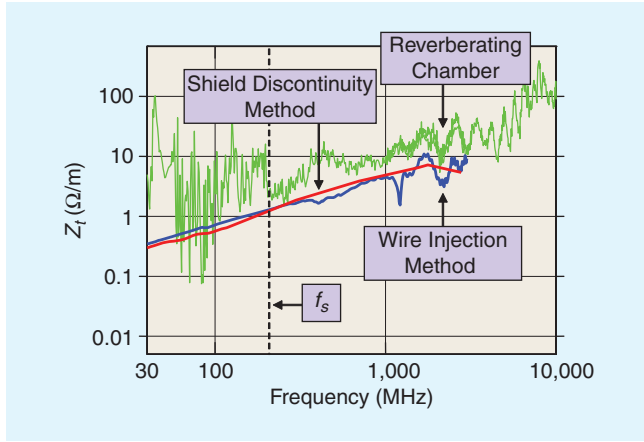


Fig. 7. Example of measurements carried out with a single braid cable of 10 cm in length, in a reverberation room (green curve), with the shield discontinuity method (red curve) and wire injection method (blue curve).

working area located above 200 MHz we can observe various amplitude fluctuations, the origin of which can be related to a combination of propagation phenomena or to leaks created by the connectors installed at the sample extremities.

As for the comparison between the measures performed on this sample by means of the shielding discontinuity method (red curve) and those performed through the injection wire method (blue curve), the frequency behaviour appears to agree when the transfer impedance amplitude obtained in the reverberation chamber is appreciably larger.

It is possible that the overestimation of the transfer impedance comes from leaks located at the level of the connectors at the sample extremities. Undeniably, contrary to usual test benches, reverberation chamber tests stress the connectors, and more specifically their back shell, with an electromagnetic field of the same level as that applied to the shielding under test. Moreover, as we have noticed for the open sample, we witness a slope change in the transfer impedance curve. This phenomenon starts at a frequency of 3 GHz.

In order to complete the previous results, the curve drawn in figure 8 represents the evolution of the shielding attenuation measured in a reverberation chamber on a RG-58 1 meter cable sample. In accordance with the definition reported in

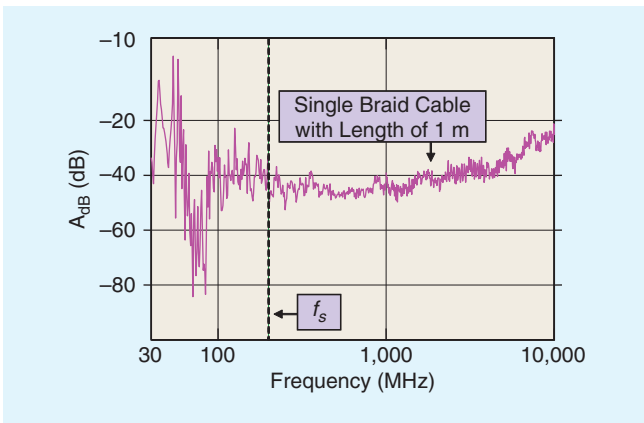


Fig. 8. RG-58 single braid coaxial cable measurement of the shield attenuation as given in equation (5).

the right hand expression of (5), the curve's vertical axis is expressed in dB.

As in the case of the previously shown curves, the attenuation characteristic very clearly highlights the reverberation chamber behaviour as it depends on whether it is located below or above  $f_s$ . In the first case the excessive amplitude of fluctuations corresponds to the mode stirrer's imperfections. Inversely, above  $f_s$ , the fluctuations are included in the uncertainty provided by the uniform statistics generated by the mode stirrer. The uncertainty must then stay within the gauge determined by the calibration procedure described in the previous section.

As far as the conversion of this curve into transfer impedance is concerned, things are more complex than on a 10 cm sample. In fact, at the lowest usable frequency of 200 MHz, the wavelength is comparable to the sample length of 1 meter and at higher frequencies this sample clearly gets oversized in relation to the wavelength. Under these conditions, the current distribution  $I_s$  on the shielding outer surface behaves as a random variable to which we can add the average value  $I_{s\text{av}}$ .

If we then bring into play the phase differences generated by propagation along the cable, the voltage collected at each matched extremities can be written as:

$$V_c = \frac{1}{2} |Z_t| \frac{1 - e^{-jk_2 \Delta L}}{jk_2} I_{s\text{av}} \quad (27)$$

In this expression, the wave number  $k_2$  is connected to the propagation speed  $v_2$  inside to the cable and to the angular frequency by means of the well known formula:

$$k_2 = \frac{\omega}{v_2} \quad (28)$$

The expression (27) immediately shows that the collected voltage will be at its maximum for those frequencies which satisfy the condition:

$$(e^{jk_2 \Delta L})_{\omega_n} = -1 \rightarrow |V_c|_{\text{maxi}} = \frac{|Z_t|}{k_2} I_{s\text{av}} \quad (29)$$

Knowing that when we measure the attenuation in a reverberation chamber we obtain the average amplitude of the power collected on the sample during a mode stirrer rotation, the largest amplitudes generated by propagation phenomena will be confused with the measurements uncertainty margins. Consequently, when the cable gets oversized in relation to the wavelength, it is advisable to correct (15) and (16) by removing the term  $\Delta L$  and by weighting with the factor  $k_2/2$ , that is:

$$|\hat{Z}_t| \cong \frac{k_2}{2} \sqrt{2Z_c Z_w} \hat{A}_{\text{lin}} \quad (30)$$

$$|\hat{Z}_t| \cong \frac{k_2}{2} \sqrt{2Z_c Z_w} 10^{+0.05 \hat{A}_{\text{dB}}} \quad (31)$$

At a close examination, the curve in figure 8, at 200 MHz and 1 GHz frequencies, reveals attenuations which are almost identical and close to  $-48$  dB. Knowing that the propagation speed inside the cable is close to  $v_2 = 2.10^8$  m/s, after having applied the correction in (31), at 200 MHz and 1 GHz we find transfer impedances of  $2.4 \Omega/\text{m}$  and  $12 \Omega/\text{m}$ , respectively. These values are then very close to the measures performed on the 10 cm sample without correction. If the shielded cable transfer impedance continuously evolves following a law proportional to the frequency, an analysis of (30) and (31) shows that the shielding

attenuation must be kept independent of frequency. Actually, the curve in figure 8 shows a rise above 1 GHz which seems to strengthen the hypothesis of an additional leakage due to the extremities connectors.

Before closing this section, it is worth indicating that above a few GHz the attenuation introduced by the cables connecting the samples to the instruments must be corrected.

## 7. Conclusion

In a previous paper [2] we have illustrated that the use of test benches based on coupled transmission lines becomes ineffective above 1 GHz. As far as frequencies significantly higher than 10 GHz are concerned, we know that extending the concept of transfer impedance to this domain is still the subject matter of fundamental questions and that is thus premature to extend its use to the whole microwave spectrum. Consequently, if we limit the extent of these conclusions to the 1 GHz–10 GHz range, the paper proves that the properties of mode stirring reverberation chambers offer interesting perspectives for the measurement of the attenuation provided by shielded cables or connectors. The issue discussed at length in the paper deals with the conversion of the shielding attenuation into a measure consistent with the transfer impedance. In section 3 it has been proven, thanks to the fields' statistical properties due to mode stirring, that the power data collected at the sample extremities are correlated to the shielding attenuation by means of a physical parameter comparable to a cable (or a connector's) transfer impedance.

In this intent, it is thus possible to calibrate the measurements by means of a sample made up of a tubular shielding fitted with a small aperture. Knowing that the transfer impedance of this device evolves through a law proportional to frequency, different tests will allow us to understand the transfer impedance behavior when the sample is irradiated by the field generated within a reverberation chamber.

From the experimental analysis detailed in section 5, we can observe that the transfer impedance measures compared to the measured values and then estimated on the test bench are fully consistent between 200 MHz and 1 GHz. The lower limit, set at 200 MHz for the minimum usable chamber frequency, allows us to observe an upper limit located around 1 GHz and characterized by an unexplained rise on the transfer impedance. Some hypotheses were formulated in order to find rational explanations to this phenomenon. One involves the legitimacy of the concept of transfer impedance when it comes to practical measures on the illumination of electromagnetic fields. Indeed, the sample's transfer impedance as it is expressed by the law proportional to the frequency drawn in (24) is not an extension of the properties of mutual inductances adopted in the transmission lines theory. It will not be surprising then if they turn out to be inaccurate in the context of practical measures of field illumination. We can also involve the contribution of other couplings generated through leakage by the azimuthal magnetic field taken into consideration only in order to set the reference formula (24). We mainly think about the influence that the other components of the magnetic field as well as the electric field exert on coupling. To these physical causes some other artifacts can be added, which are generated by parasitic couplings occurring on the sample connectors exposed to the field surrounding the chamber.

As for the other tests performed on a cable sample made up of a single braid shielding which has shown a similar behavior, we can say that a lot of work has still to be done in order to understand the concept of transfer impedance in the micro-waves domain.

## References

- [1] B. Démoulin, L. Koné, *Shielded Cable Transfer Impedance Measurements* IEEE-EMC Newsletter, Fall 2010, pp 30–37.
- [2] B. Démoulin, L. Koné, *Shielded Cable Transfer Impedance Measurements High frequency range 100 MHz – 1 GHz*, IEEE-EMC Newsletter, Winter 2011, pp 8–16.
- [3] L. Martens, A. Madou, B. Vanlandschoot, L. Koné, B. Démoulin, P. Sjöberg, A. Anton, L. Van der Torren, J. Van Koetsem, H. Hoffmann and U. Sthricker, *Shielding Of Backplane Interconnection Technology Systems (EU SOBITS project)* IEEE Transactions on EMC, Vol. 42, N°4, November 2000, pp. 427–440.
- [4] M.L. Crawford, J.M. Ladbury, *Modes Stirred Reverberation Chambers of cables and Connectors, an Assessment of MIL-STD-1344A Method 3008*, Proceeding of the IEEE International symposium on EMC, pp 30–36, August 1988.
- [5] D.A. Hill, M.L. Crawford, M.L. Kanda, D.L. Wu, *Aperture Coupling to a Coaxial Air Line: Theory and Experiment* IEEE Transactions on EMC, Vol. 35, N°1, pp 69–74, February 1993.
- [6] K.S.H. Lee, C. Baum, *Application of Modal Analysis to Braided Shielded Cables* IEEE Transactions on EMC, Vol. 17, N°3, pp 159–169, August 1975.
- [7] P. Corona, P. Ladbury, J. Latmirel, *Reverberation Chamber Research Then and Now: A review of Early Work and Comparison with current Understanding* IEEE Transactions on EMC, Vol. 44, N°1, pp 87–94, February 2002.
- [8] F. Broydé, E. Clavelier *Comparison of Coupling Mechanisms on Multiconductors Cables* IEEE Transactions on EMC, Vol. 35, N°4, pp 409–416, November 1993.
- [9] Y. Bourri, *Analyses Physiques et Simulations Numériques Appliquées à l'Evaluation des Fuites Electromagnétiques des Connecteurs Blindés* PhD Thesis, Université de Lille, 2009.
- [10] D.A. Hill, *Electromagnetic Fields in Cavities* IEEE Press series on Electromagnetic Wave Theory, Wiley 2009.
- [11] B. Démoulin, P. Besnier *Les Chambres Réverbérantes en Electromagnétisme* Editions Hermès Lavoisier, 2010.
- [12] B. Eicher, L. Boillot *Very Low Frequency to 40 GHz Screening Measurements on Cables and Connectors; Line Injection Method and Mode Stirred Chamber* IEEE International Symposium on EMC, Anaheim, CA, USA, August 1992 Symposium record, DOI: 10.1109 / ISEMC.1992.626099, pp 302–307.

## Biography



**Bernard Démoulin** was born in 1946. He received his Ph.D. degree in 1981 and until 2008 was the head of the EMC group at the IEMN-TELICE Laboratory. He is presently professor emeritus at the University of Lille, France. His domain of expertise is mainly related to the effect of electromagnetic coupling through cables, transfer impedance measurement and the study of mode stirred reverberation chambers. He is a senior member of the French Society of Electrical Engineers (SEE) and a corresponding member of URSI.



**Lamine Koné** was born in 1956. He received his Ph.D. degree in 1989. Since 1990, he has been working as an engineer at the IEMN-TELICE laboratory at the University of Lille, France. His domain of expertise deals with EMC measurements, especially involving the transfer impedance on shielded cables or connectors and tests carried out in mode stirred reverberation chambers.

EMC